Journal of Physics Communications

PAPER

# Passively mode-locked ultrashort pulse fiber laser incorporating multi-layered graphene nanoplatelets saturable absorber

**K Y Lau**[1], **N H Zainol Abidin**[1], **M H Abu Bakar**[1], **A A Latif**[2], **F D Muhammad**[2], **N M Huang**[3], **M F Omar**[4] and **M A Mahdi**[1]

[1] Wireless and Photonics Network Research Centre, Faculty of Engineering, University Putra Malaysia, 43400 UPM Serdang, Selangor, Malaysia
[2] Department of Physics, Faculty of Science, Universiti Putra Malaysia, 43400 UPM Serdang, Selangor, Malaysia
[3] Faculty of Engineering, Xiamen University of Malaysia, Jalan Sunsuria, Bandar Sunsuria, 43900 Sepang, Selangor Darul Ehsan, Malaysia
[4] Physics Department, Faculty of Science, Universiti Teknologi Malaysia, 81310 Skudai, Johor, Malaysia

**E-mail:** mam@upm.edu.my

**OPEN ACCESS**

**RECEIVED**
16 May 2018

**REVISED**
11 June 2018

**ACCEPTED FOR PUBLICATION**
20 June 2018

**PUBLISHED**
5 July 2018

**Keywords:** mode-locked lasers, graphene, saturable absorbers, ultrafast nonlinear optics



## Abstract

In this paper, a passive mode-locked erbium-doped fiber laser (EDFL) incorporating graphene nanoplatelet (GNP) powder-based saturable absorber (SA) with short pulse duration in femtosecond range is demonstrated. A good synthesis of GNP can be simply produced via a combination of thermal, chemical, and mechanical exfoliation of expandable graphite. The GNP-SA is fabricated by mechanically imprinting the powder onto the tip of a single mode fiber ferrule. The characterization of SA is done via focus ion beam scanning electron microscope, energy dispersive X-ray spectroscopy, as well as Raman spectroscopy. The fabricated GNP-SA has 1.8 % modulation depth and C-band transmission loss of less than 1.8 dB. The ring-configuration EDFL integrated with GNP-SA yields a mode-locking threshold of 22.6 mW pump power. Net anomalous dispersion of the laser cavity is validated by the observation of Kelly's sideband in the optical spectrum. At maximum pump power of 115.8 mW, the mode-locked EDFL has a pulse repetition rate of 13.11 MHz, $\text{sech}^2$ profile fitted pulse duration of 694 fs, peak-to-pedestal extinction ratio of 58.2 dB, average output power of 6.7 mW, and pulse energy of 507.2 pJ. Our proposed GNP-SA is feasible as a mode-locker for ultrashort pulsed fiber laser with advantage in terms of simple synthesis and fabrication technique.

## 1. Introduction

Recent fiber laser technologies have highlighted the significance of passively mode-locked ultra-short pulse in multiple applications such as medical field [1], molecular science [2], astrophysics [3], and high energy laser system [4]. The phrase 'mode-locking' is defined as multiple axial modes being locked together in a laser cavity [5]. The resonance is observed for any mode-locking phenomenon in which pulse radiation is generated by coherent phase matching between different modes. The ultrashort pulse generation can be achieved by either active or passive mode-locking techniques. The latter technique is favorable due to simple operation that does not require an external modulator.

Saturable absorber (SA) is generally utilized for the generation of passively mode-locked fiber laser due to its intensity-dependent optical loss, which reduces at higher light intensity. This phenomenon can be observed when all possible initial states are depleted and the final states are partially occupied in conjunction to Pauli's blocking effect. The fiber-integrated SA was demonstrated in the past few years using several types of nanomaterials. These nanomaterials include transition metal dichalcogenides [6, 7], topological insulator [8], black phosphorus [9], carbon nanotube [10] and graphene [11]. Among these various nanomaterials, graphene is preferred due to its ultra-broadband operating spectral range and gapless linear dispersion of Dirac-electrons near the Fermi energy [12]. Graphene has a honeycomb lattice structure which is formed by $sp^2$ hybridized carbon atoms in planar configuration [13] with a constant presence of electron-hole pair in resonance [14].

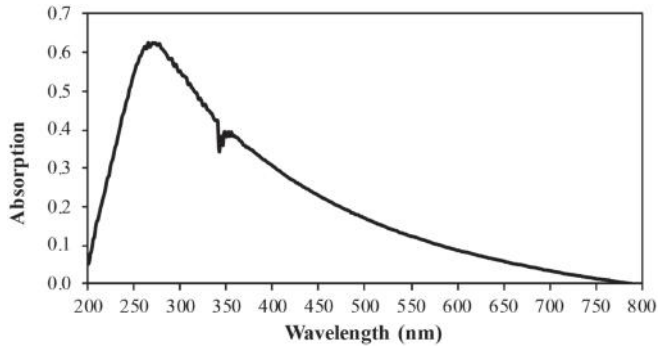


**Figure 1.** UV-visible absorption spectrum of the synthesized GNP powder.

Therefore, the optical inter-band transition is independent of frequency and corresponds solely to the optical conductance of photon energies [13].

Graphene can be tailored into several forms such as monolayer graphene, graphene oxide and graphene nanoplatelet (GNP). Based on [15], monolayer graphene is complicated and expensive to fabricate SA due to the synthesizing and imprinting procedures. On the other hand, graphene oxide has high defect density which could contribute to the deposition loss as high as ~7 dB [16]. The GNP typically exists in the stacking of multiple single layers of graphene [17]. The modulation depth of GNP is improved by such stacking properties. Therefore, GNP offers this slight advantage as one of promising SA candidates. The mode-locked erbium-doped fiber laser (EDFL) using GNP-SA has been reported with ultrashort optical pulses of 1.67 ps [18] and 1.9 ps [15]. The deposition method of GNP on the fiber ferrule is based on mechanical imprinting technique. In addition, another SA fabrication method was investigated by embedding GNP in photonics crystal fiber (PCF), which improved the pulse duration to 650 fs [19]. Nevertheless, the fabrication process of depositing GNP into 3.1 $\mu$m hole diameter is complicated.

In this paper, GNP is used for the fabrication of sandwiched-type SA through mechanical imprinting on fiber ferrule. The optimization of GNP thickness is controlled through mechanical exfoliation technique using a Scotch tape. We demonstrate a sandwich-structured GNP-SA which generates shorter pulse duration of 694 fs compared to previous GNP-SA mode-locked EDFL using similar SA structure [15, 18]. In addition, this work highlights the feasibility of GNP-SA to generate femtosecond mode-locked pulse laser through simple SA fabrication procedures.

## 2. Synthesis of GNP powder

GNP powder is synthesized from expandable graphite (3772, Asbury Carbons, Inc.) based on slight modification of the procedures in [20]. The expandable graphite is first subjected to thermal exfoliation inside an oven at a temperature of 950 °C for 10 s. In order to further exfoliate the expanded graphite, 0.1 g of the expanded fluffy powder is then soaked in 100 ml mixture of sulphuric acid ($V(H_2SO_4)$) and nitric acid ($V(HNO_3)$) with ratio of 1:1 for 24 h. After that, the treated expanded graphite is washed with deionized water for 10 times through centrifugation method to remove excess acids. Finally, the treated expanded graphite is ultrasonicated in ethanol solution (0.1 mg $ml^{-1}$) using probe sonicator (QSonica Q700) for further exfoliation. The sonicated sample is centrifuged at 5000 rpm and the precipitate is dried in the oven at 60 °C for 12 h to obtain solvent-free GNP powder.

A UV-visible spectrum analyzer is utilized to characterize the synthesized GNP powder as depicted in figure 1. The spectrum shows a broad absorption band with a peak at 264 nm and a shoulder at approximately 345 nm. The 264 nm peak confirms that the GNP has a graphitic structure. On the other hand, the 345 nm shoulder observed is due to the excitation of $\pi$-plasmon. The wavelength of the shoulder is slightly shifted compared to other reported graphene absorption spectra due to the stretching of the bonds [21]. Furthermore, the state of the GNP can be conjectured to be multi-layered based on the prominence of the 345 nm shoulder.

## 3. Fabrication and preparation of GNP-SA

The preparation steps of GNP-SA are illustrated in figure 2. First, a small amount of GNP powder is taken with a spatula and placed on a clean filter paper as portrayed in figure 2(a).

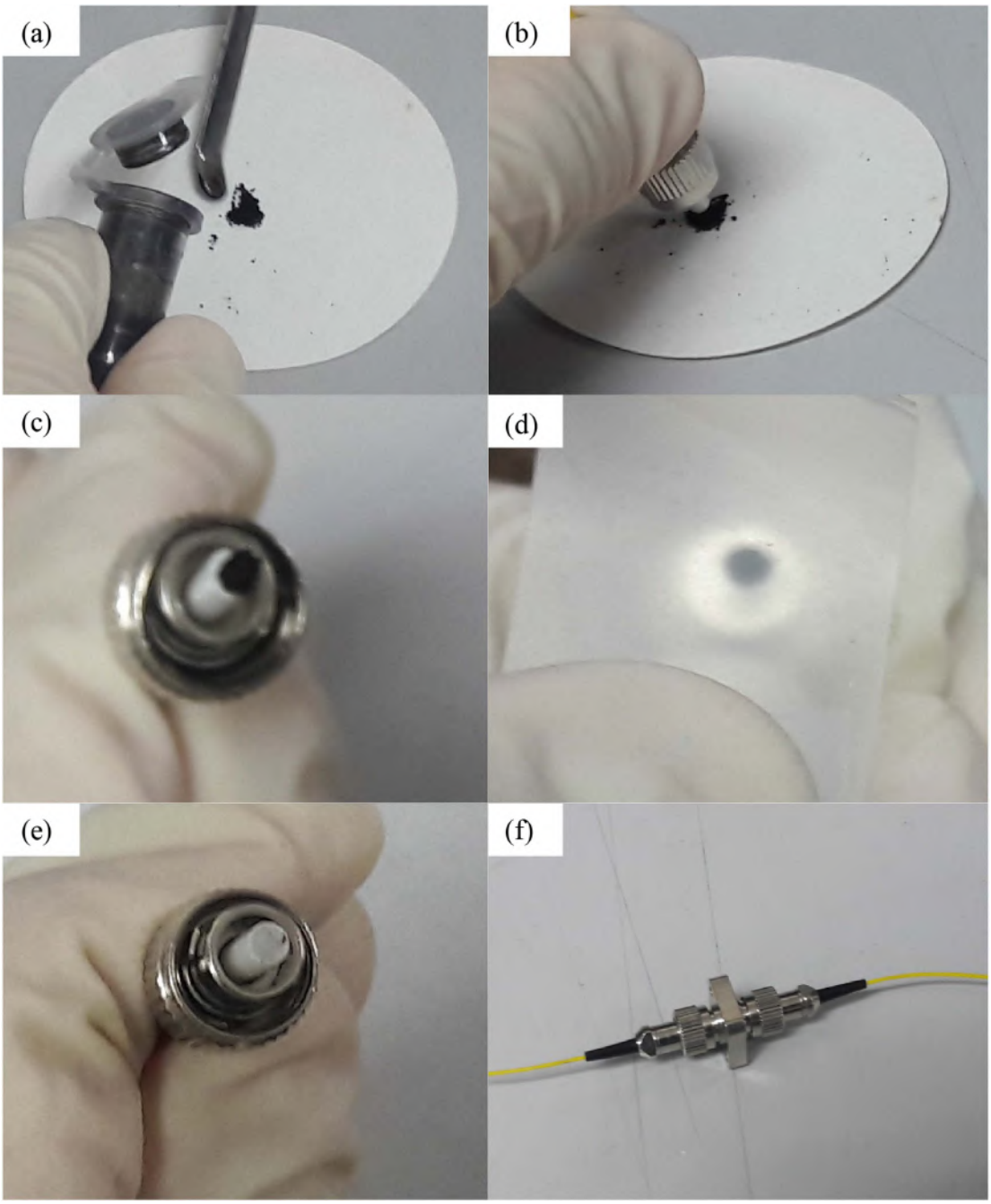


**Figure 2.** Fabrication procedures of GNP-SA.

A FC/PC SMF-28 fiber ferrule is then dipped into the GNP powder (figure 2(b)) allowing the adsorption of GNP powder with uneven thickness as presented in figure 2(c). A clean scotch tape is then used to exfoliate the deposited GNP powder several times (figure 2(d)) in order to obtain a better distribution of GNP powder and the least number of layers as possible, shown in figure 2(e). Lastly, The GNP powder-deposited fiber ferrule is attached to a different fiber ferrule to assemble the SA as depicted in figure 2(f).

### 3.1. Morphology analysis

A closer look at the GNP-imprinted fiber ferrule after mechanical exfoliation process is realized using Oxford Instrument's X-Max$^N$ focus ion beam scanning electron microscope (FIB-SEM) with different magnification size as illustrated in figure 3. Figure 3(a) illustrates the FIB-SEM image of the fiber ferrule taken with magnification size of 1500. The outer circle with diameter of 125 $\mu$m denotes the fiber cladding region. On the other hand, the smaller circle with 9.8 $\mu$m diameter measurement illustrates the fiber core region that is extensively covered with GNP. This fiber core region is further analyzed by adjusting the magnification size of FIB-SEM to 10 000 as depicted in figure 3(b). Based on this figure, clusters of GNP sheets are observed.

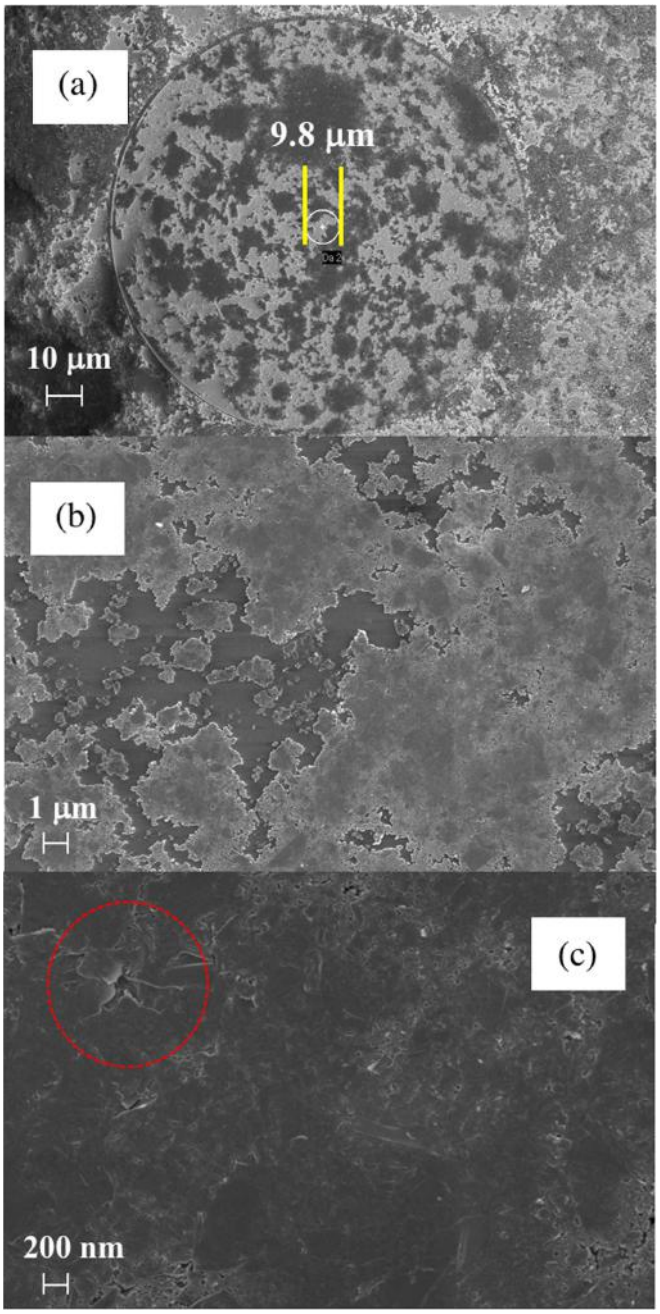


**Figure 3.** FIB-SEM images of imprinted GNP on the fiber ferrule observed with magnification size of (a) 1500×, (b) 10 000× and (c) 50 000×.

Figure 3(c) depicts a random chosen spot within the fiber core observed at magnification size of 50 000. A crack in the material can be detected (circled in red), which can spontaneously happen as the GNP sheets harden.

### 3.2. Elemental analysis

The material distribution of GNP on the fiber core is identified and mapped using Oxford Instruments X-Max$^N$ 80 energy dispersive X-ray (EDX) spectroscopy as shown in figure 4. This measurement is taken using 1 kV acceleration voltage to distinguish only the graphene material and to minimize the interaction between electrons and optical fiber. Figure 4(a) shows the combination of carbon (C) and oxygen (O) elements which are represented by red dots (figure 4(b)) and green dots (figure 4(c)), respectively. The dashed circle with diameter measurement of 9.8 $\mu$m in figure 4(a) denotes the fiber core region, which is covered with a large amount of GNP. The basic chemical composition of GNP is only carbon. Hence, the regions with the abundance of C spots exhibit minimal presence of O spots, and vice versa. The lack of C element in some regions is likely due to the exfoliation process.

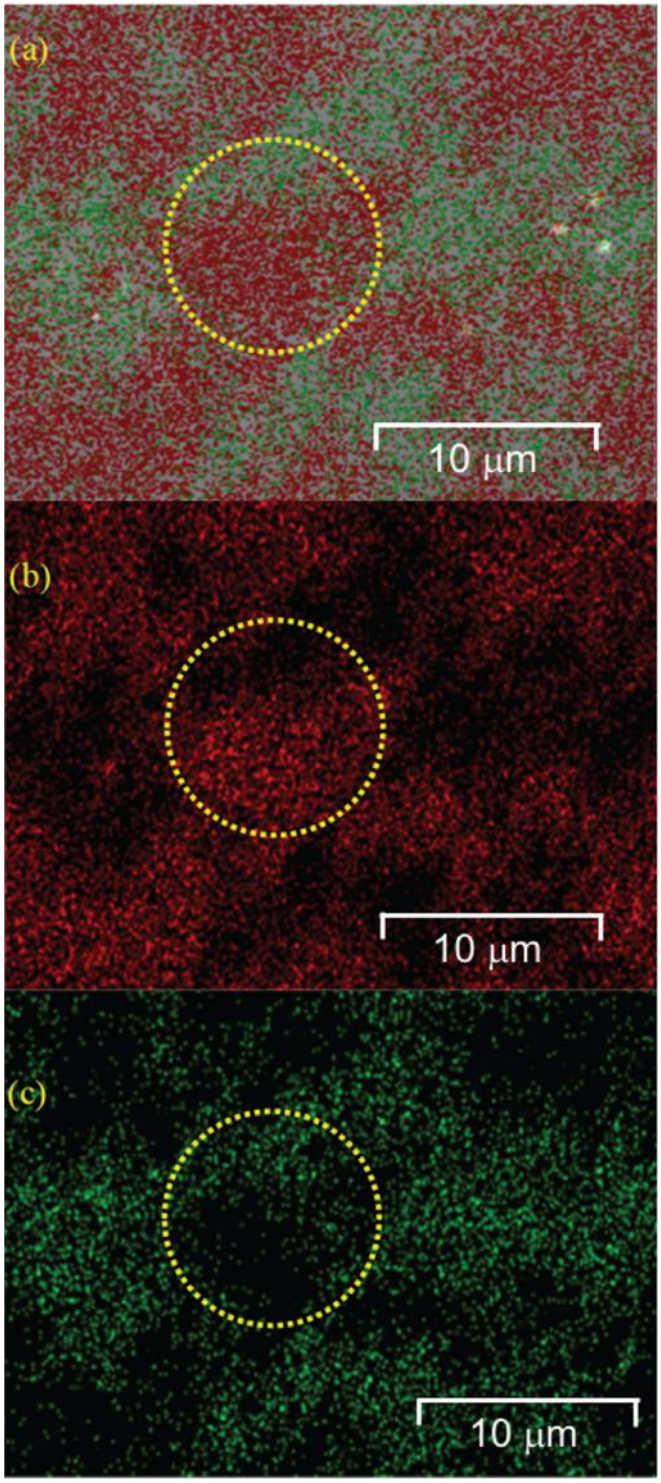


**Figure 4.** Material distribution images measured from EDX of imprinted GNP on fiber ferrule for (a) combination of carbon and oxygen elements, (b) carbon element and (c) oxygen element. The dashed circle in yellow denotes the fiber core region.

The EDX spectrum corresponding to figure 4 is illustrated in figure 5. Based on the spectrum, only C and O elements are detected within the fiber core region area. The O element is detected from silicon dioxide ($SiO_2$) material in the optical fiber. However, the presence of Si element cannot be observed since the acceleration voltage of 1 kV used is below than the peak of $Si_{K\alpha}$ at 1.7 keV. Furthermore, the $Si_{L\alpha}$ peak at 0.093 keV also cannot be observed because the EDX system is only able to detect X-ray energy for Beryllium ($Be_{K\alpha}$) which is 0.108 keV and above. Therefore, the high purity of C from graphene is proved based on the absence of other chemical elements observed from the EDX spectrum.

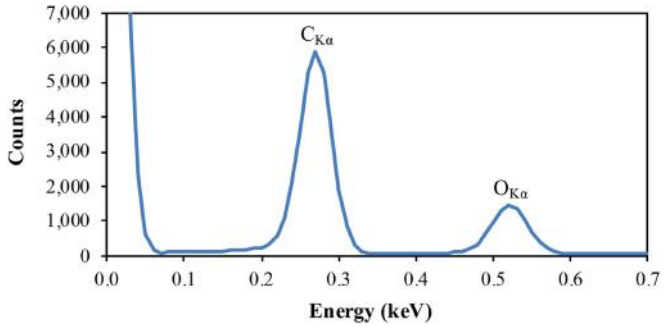


**Figure 5.** EDX spectrum of imprinted GNP on the fiber core.

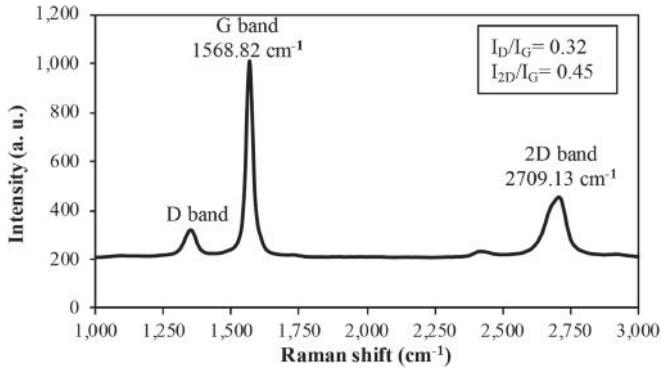


**Figure 6.** Raman spectrum of imprinted GNP on the fiber core.

### 3.3. Raman spectrum

To measure the defect density and to quantify the graphene layers, a WITec Raman spectroscopy (Alpha 300R) with 487.9 nm excitation wavelength is employed. The Raman spectrum of the deposited GNP is shown in figure 6. The D band at 1350.03 $cm^{-1}$ and G band at 1568.82 $cm^{-1}$ represent the visible excitation of carbons [22]. In the $sp^2$ hybridized carbon atoms, the G band is a direct relation to bond stretching in the chains and rings, while the D band represents the breathing modes in the rings [23, 24]. Using the intensity ratio between the D peak and G peak ($I_D/I_G$), the defect density of the GNP is calculated to be 0.32. The low defect density can be credited to the good synthesis process that minimizes the formation of graphene oxide [25].

The Raman spectrum also shows the 2D band at wavelength 2709.13 $cm^{-1}$, which is the 2nd-order Raman scattering of the D band. This would explain the twice in shifting rate to the D-band [26]. The 2D band is actually contributed by two opposite momentum phonons in the highest optical branch with the wave vectors nearing the Brillouin zone κ point [20]. Additionally, using the visual comparison of the 2D peak to the G peak, one can deduce the state of the graphene whether it exists as a single sheet or multiple sheets [27]. A G peak with higher intensity in comparison to the 2D peak denotes that the deposited GNP exists in multilayer form while the opposite case would hold true if the sample occurred as a single sheet. However, to exactly quantify this, the intensity ratio of 2D band to G band ($I_{2D}/I_G$) is calculated, and amounted to a ratio of less than two. A ratio of less than two confirms the multi-layered state of the deposited GNP speculated earlier.

## 4. Optical characterization of GNP-SA

Subsequently, the transmission loss of the proposed GNP-SA is characterized. To perform this characterization, the GNP-SA is connected to an amplified spontaneous emission (ASE) source and an optical spectrum analyzer (OSA) to capture the transmission. Prior to this, the transmission spectrum of the ASE source is acquired. The transmission loss is calculated through the difference in transmission spectra with and without GNP-SA. The resulting loss spectrum is shown in figure 7, which exhibits value below 1.8 dB across the C-band wavelength region.

Next, the modulation depth (MD) of the GNP-SA is measured. The assessment of the modulation depth can be obtained using a graph of normalized absorbance versus peak intensity. Accordingly, the setup for the

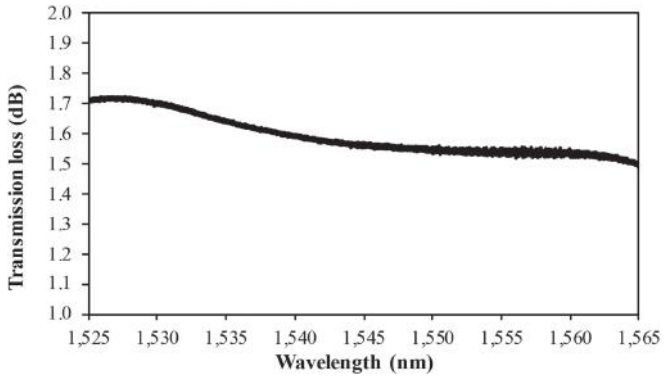


**Figure 7.** Transmission loss of GNP-SA over C-band wavelength region.

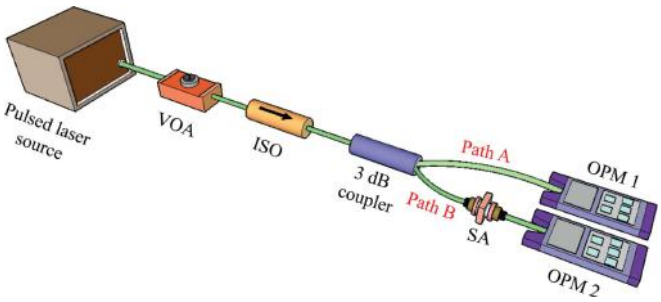


**Figure 8.** GNP-SA non-linear saturable absorption characterization setup.

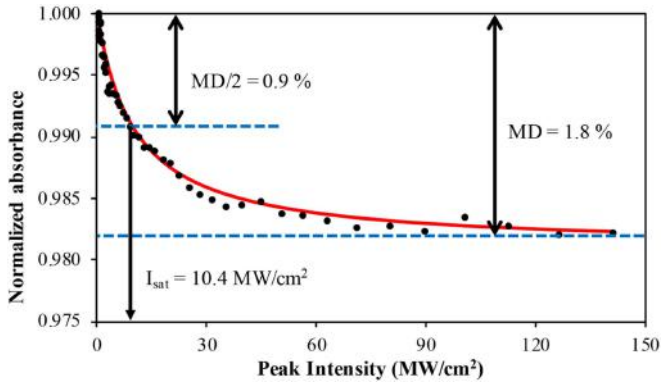


**Figure 9.** GNP-SA power dependent nonlinear saturable absorption curve.

nonlinear-saturable absorption characterization is presented in figure 8. The setup consists of a variable optical attenuator (VOA) that tunes the launched power of the pulsed laser source. The operating wavelength of the M-Fiber MenloSystems pulsed laser source is 1550 nm with pulse duration and repetition rate of 117 fs and 250 MHZ, respectively. An isolator is placed in between the VOA and a 3 dB optical coupler to prevent back-reflection. The 3 dB optical coupler channels the optical signal into Path A and Path B equally. Two optical power meters OPM1 and OPM2, are employed to measure the reference power measurement from Path A and the power-dependent transmission measurement from Path B, respectively.

The nonlinear saturable absorption curve of the GNP-SA with peak intensity variation is plotted in figure 9. Based on the evaluation of the normalized absorbance graph, the MD obtained is 1.8 %. It can be expected that the proposed GNP-SA will be able to self-start the mode-locked laser operation as the MD is higher than the one reported in [16]. Subsequently, the non-saturable loss ($\alpha_{ns}$) and saturation intensity ($I_{sat}$) that can be approximated based on the same graph are 37 % and 10.4 MW cm$^{-2}$, respectively. The stacking of the GNP in the proposed SA contributed to the high non-saturable loss. However, the $\alpha_{ns}$ of our GNP-SA is similar to the

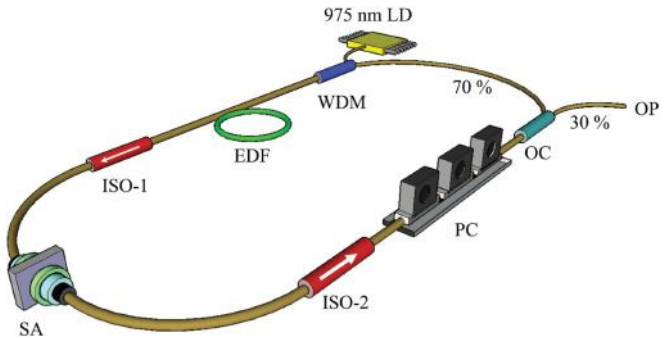


**Figure 10.** Experimental setup of mode-locked EDFL with GNP-SA.

graphene-SA reported in [28]. The proposed SA has a rather low saturation intensity which can only be obtained when the material has a low defect density [29]. This is in contrast to the graphene-SA presented in [30], which reported a high saturation intensity of 65 MW $cm^{-2}$ due to high material defect density. Low saturation intensity is highly desirable in SAs as it can assist in obtaining a low threshold condition in mode-locked lasers [31].

## 5. Experimental setup of mode-locked fiber laser

The experimental setup of a mode-locked EDFL employing the GNP-SA is shown in figure 10. A 975 nm laser diode (LD) pumps a 7 m HP980 erbium-doped fiber (EDF) via a 980/1550 nm wavelength division multiplexer (WDM). The EDF has a dispersion coefficient of −18 ps $nm^{-1}$ $km^{-1}$ at 1550 nm and absorption coefficients ranging from 3.5 dB $m^{-1}$ to 5.5 dB $m^{-1}$ for 1530 nm to 1550 nm wavelengths. The GNP-SA is connected to the other end of the EDF, and isolators (ISO-1 and ISO-2) are in inserted just before and after the GNP-SA to ensure unidirectional pulse propagation as well as to prevent back-reflections into the GNP-SA. The back-reflections may originate from backward EDF ASE which can instigate multiple-reflections degrading the laser stability. A polarization controller (PC) is connected to ISO-2 to tune the polarization state and to reduce cavity birefringence effect. A 70:30 optical coupler (OC) is connected to the output of the PC, with the 70% leg completing the ring cavity back into the 980/1550 WDM. Meanwhile, the 30% leg is used as the output port for signal analysis.

## 6. Mode-locked fiber laser performance

Figure 11 shows the spectral measurement of the mode-locked EDFL incorporating GNP-SA with pump power variation. Initially, the setup generates a continuous wave (CW) laser at 18.1 mW pump power. Increasing the pump power to 22.6 mW, resulted in the attainment of the mode-locked laser threshold condition. However, from 43.9 mW to 67.4 mW pump power, a distinct peak at wavelength 1558.28 nm appeared which indicates that the operation has switched from mode-lock to CW. This shows that the mode-locked laser has not yet reached stable operation. Beyond 67.4 mW, the CW signal is suppressed securing a stable seed laser source for mode-locking operation. The mode-locked laser spectrum is then well maintained beyond 67.4 mW up to the maximum pump power of 115.8 mW. The central wavelength of the mode-locked laser is 1558.35 nm with a 3 dB bandwidth of 4.21 nm.

Additionally, from the spectrum in figure 11, Kelly's sidebands are observed which is a clear indication that the laser operates within the net anomalous dispersion of conventional soliton regime [32]. A soliton regime manifests from the interplay between negative dispersion and the nonlinear effect in the laser cavity, as a result of balanced effect between dispersion and non-linearity in the laser cavity [33]. The total group velocity dispersion (GVD) is calculated to verify that the laser performs in the net anomalous dispersion regime. The total measured length of the laser cavity is 22.9 m and consists of Corning SMF-28, Corning Hi-1060 SMF, and Lucent Technologies HP980 EDF. The dispersion coefficient, $\beta_2$ at 1550 nm for each fiber type are shown in table 1. The total GVD contributed by each fiber type is then calculated by multiplying its length with the dispersion coefficient. Summing up the total GVD from each fiber type, the net GVD of the entire cavity is −0.2313 $ps^2$, which places the laser cavity in net anomalous dispersion regime.

The pump power is then fixed at 115.8 mW for optical pulse analysis. The pulse repetition rate is measured by Tektronix TDS 3012C digital phosphor oscilloscope through a 5 GHz Thorlabs SIR5-FC InGaAs FC/PC-coupled photodetector. Figure 12 shows the measured output pulse train. From this finding, the pulse repetition

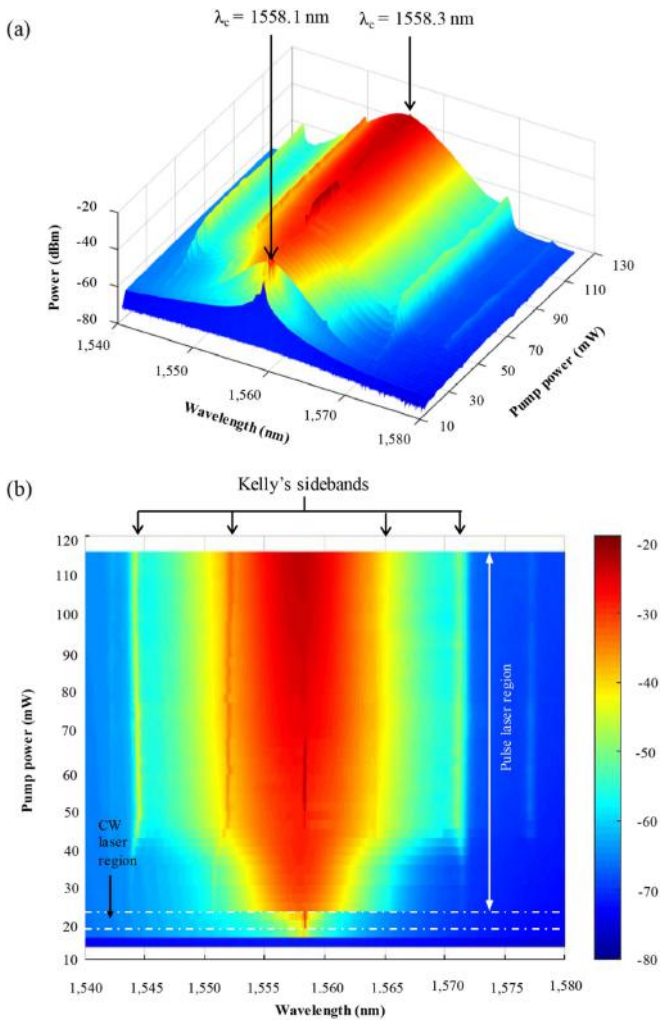


**Figure 11.** Optical spectrum of the mode-locked EDFL.

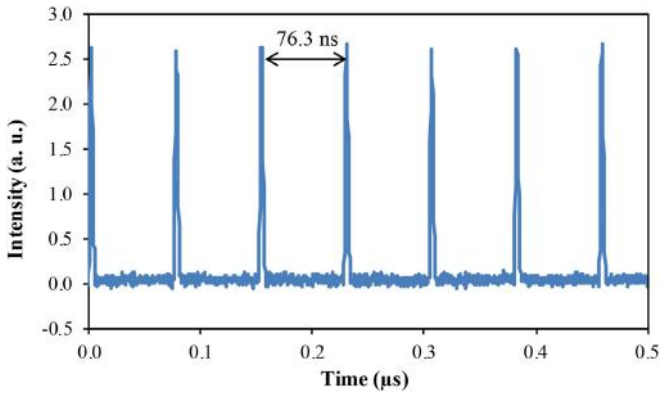


**Figure 12.** Output pulse train of the mode-locked EDFL.

**Table 1.** Estimated values of the GVD for each type of optical fiber for the entire EDFL cavity.

| Fiber type | L (m) | $\beta_2$ (ps$^2$/km) | Net GVD (ps$^2$) |
|---|---|---|---|
| SMF-28 | 14.9 | −22 | −0.3278 |
| Hi-1060 | 1 | −7 | −0.0070 |
| EDF | 7 | 23 | 0.1035 |

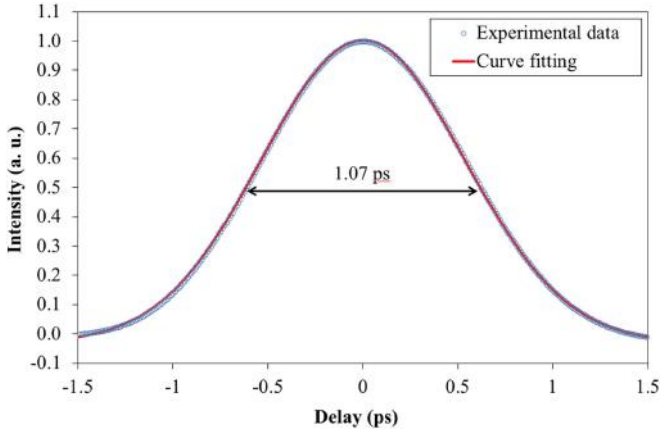


**Figure 13.** Autocorrelator trace of the mode-locked EDFL.

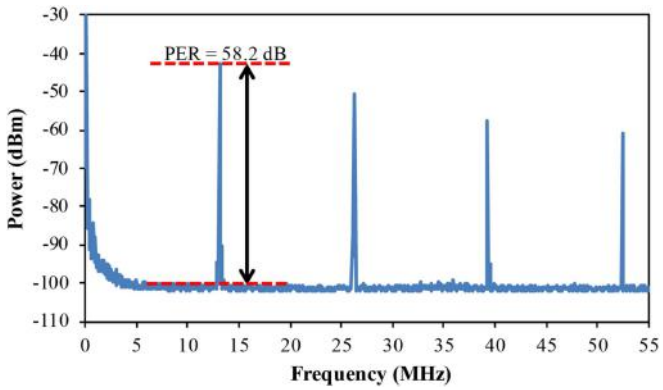


**Figure 14.** PER measurement of the mode-locked EDFL.

rate is 13.11 MHz based on the response time of 76.3 ns. The constant pulse repetition rate featured by the mode-locked laser is favorable over situations where a slight fluctuation in the gain medium lifetime and pump power easily changes the repetition rate, such as in a Q-switched laser [34]. The mode-locked laser pulse repetition rate is in agreement with the round-trip time. The absence of multiple-pulsing and parasitic Q-switching instabilities establishes the high stability of this mode-locked laser [35].

The autocorrelation trace for the mode-locked laser is presented in figure 13. The trace is captured by APE PulseCheck autocorrelator. From the figure, the absence of pedestal indicates that the pulse operates neither in bound-soliton regime [36] nor flow of soliton [37]. Therefore, the generated pulse is of high quality. The autocorrelation pulse duration ($\tau_{ac}$) is measured to be 1.07 ps. The pulse conforms to the sech$^2$ profile and has a full-width at half-maximum pulse duration ($\tau_{FWHM}$) of 694 fs that is obtained by multiplying $\tau_{ac}$ with the deconvolution factor of sech$^2$ profile (0.648). This value is shorter that the one reported in [15, 18]. The estimated time bandwidth product (TBP) from the experimental result is 0.36 which is higher than the 0.315 value of the sech$^2$ pulse at the transform-limit. It is possible that the difference is caused by minor chirping, that exists because of residual cavity dispersion [38]. The chirped optical pulse possesses longer pulse width compared to an ideal sech$^2$ optical pulse. Therefore, by balancing the residual cavity dispersion [39] or utilizing an SA with higher modulation depth [40], one can expect a shorter pulse width that will lead to a TBP value closer to the transform-limited one.

The frequency spectrum of the fundamental pulse is shown in figure 14. The frequency spectrum is taken using GW Instek GSP-830 electrical spectrum analyzer. From the spectrum, the stability of the pulse train can be evaluated through the measurement of peak-to-pedestal extinction ratio (PER) of the frequency signal. In this measurement, the frequency domain is set to a span of 55 MHz with a 300 Hz resolution bandwidth. A PER value of 58.2 dB is obtained which confirms a good pulse train stability [28].

Figure 15 shows the average output power and pulse energy of the mode-locked laser as a function of pump power. The pulse energy is calculated by the ratio of the average output power to the pulse repetition rate. With increasing pump power, a linear trend is presented for both the average output power and the pulse energy. As

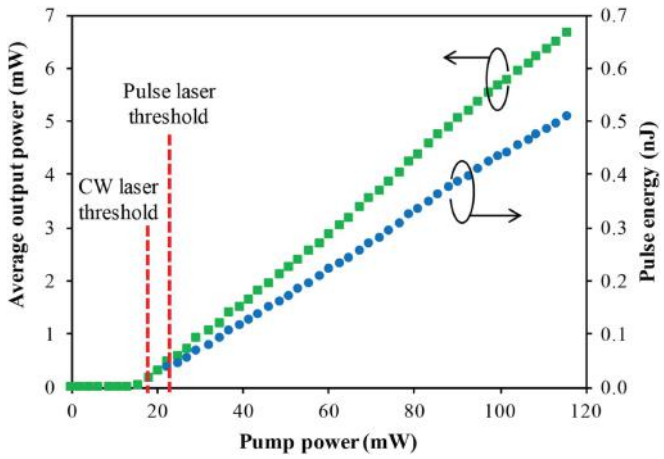


**Figure 15.** Average output power and pulse energy as a function of pump power.

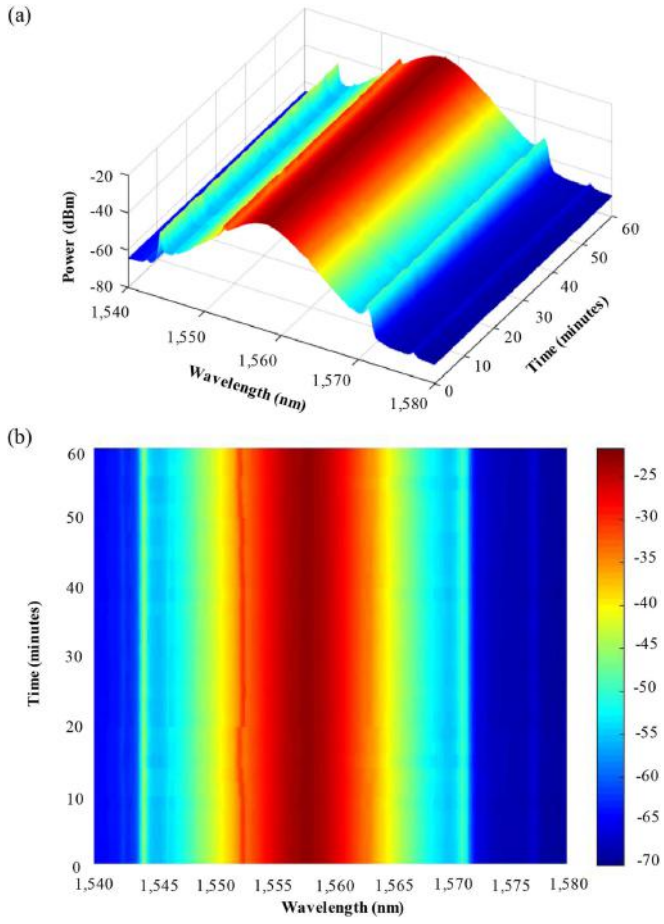


**Figure 16.** Average output power and pulse energy as a function of pump power.

the pump increases from the minimum to the maximum pump power, a growth from 0.5 mW to 6.7 mW is observed for the average output power while the pulse energy rises from 34.3 pJ to 507.2 pJ. The increment rate for the average output power and pulse energy are approximately 0.67 mW and 50.74 pJ, respectively for every 10 mW increase in pump power.

Figure 16 shows the stability measurement of the output spectrum for the GNP-SA based mode-locked EDFL. The output spectrum is recorded every 2 min for a short-term stability measurement within one hour observation period at 115.8 mW pump power. Minimal deviation is observed within the period for both

1558.35 nm central wavelength and −22.7 dBm peak output power, confirming the stability of this GNP-SA based mode-locked EDFL.

## 7. Conclusions

In conclusion, a passive mode-locked EDFL in soliton regime is demonstrated by incorporating GNP-SA. The pulse duration obtained at FWHM is 694 s, placing the scheme in the femtosecond laser category. The mode-locked generation was achieved at 22.6 mW pump power and has a central wavelength of 1558.35 nm with 3 dB spectral width of 4.21 nm. The operation of the mode-locked EDFL in the net anomalous dispersion regime is confirmed through the manifestation of Kelly's sidebands in the spectral output. At the maximum pump power of 115.8 mW, the measurements obtained for the average output power, pulse energy, and pulse repetition rate are 6.7 mW, 507.2 pJ, and 13.11 MHz, respectively. This work highlights the simplicity and feasibility of GNP as saturable absorption material for mode-locked EDFL. The high-quality femtosecond pulse output generated in this work encourages future investigation of this GNP-SA in terms of its long-term reliability for generating stable optical pulses.

## Acknowledgments

This work was supported in part by the Ministry of Higher Education, Malaysia (GP-IPB/2014/9440700) and Royal Society-Newton-Ungku Omar Advanced Fellowship (NA150463).

## ORCID iDs

M A Mahdi https://orcid.org/0000-0002-2843-181X

## References

[1] Fernandez E J, Hermann B, Povazay B, Unterhuber A, Sattmann H, Hofer B, Ahnelt P K and Drexler W 2008 Ultrahigh resolution optical coherence tomography and pancorrection for cellular imaging of the living human retina *Opt. Express* **16** 11083–94
[2] Stowe M C, Pe'er A and Ye J 2006 High resolution atomic coherent control via spectral phase manipulation of an optical frequency comb *Phys. Rev. Lett.* **96** 153001
[3] Li C-H, Benedick A J, Fendel P, Glenday A G, Kärtner F X, Phillips D F, Sasselov D, Szentgyorgyi A and Walsworth R L 2008 A laser frequency comb that enables radial velocity measurements with a precision of 1 $cms^{-1}$ *Nature* **452** 610–2
[4] Kim J, Cox J A, Chen J and Kärtner F X 2008 Drift-free femtosecond timing synchronization of remote optical and microwave sources *Nat. Photon.* **2** 733–6
[5] Haus H A 2000 Mode-locking of lasers *IEEE J. Sel. Top. Quantum Electron.* **6** 1173–85
[6] Liu M, Cai Z R, Hu S, Luo A P, Zhao C J, Zhang H, Xu W C and Luo Z C 2015 Dissipative rogue waves induced by long-range chaotic multi-pulse interactions in a fiber laser with a topological insulator-deposited microfiber photonic device *Opt. Lett.* **40** 2667–70
[7] Luo A-P, Liu M, Wang X-D, Ning Q-Y, Xu W-C and Luo Z-C 2015 Few-layer $MoS_2$-deposited microfiber as highly nonlinear photonic device for pulse shaping in a fiber laser *Photonics Res.* **3** A69–78
[8] Yan P, Lin R, Ruan S, Liu A, Chen H, Zheng Y, Chen S, Guo C and Hu J 2015 A practical topological insulator saturable absorber for mode-locked fiber laser *Sci. Rep.* **5** 8690
[9] Li J, Luo H, Zhai B, Lu R, Guo Z, Zhang H and Liu Y 2016 Black phosphorus: a two-dimension saturable absorption material for mid-infrared Q-switched and mode-locked fiber lasers *Sci. Rep.* **6** 30361
[10] Martinez A, Araimi M A, Dmitriev A, Lutsyk P, Li S, Mou C, Rozhin A, Sumetsky M and Turitsyn S 2017 Low-loss saturable absorbers based on tapered fibers embedded in carbon nanotube/polymer composites *APL Photonics* **2** 126103
[11] Zapata J D, Steinberg D, Saito L A M, de Oliveira R E P, Cardenas A M, Thoroh E A and De Souza E T 2016 Efficient graphene saturable absorbes on D-shaped optical fiber for ultrashort pulse generation *Sci. Rep.* **6** 20644
[12] Hasan T, Sun Z P, Wang F Q, Bonaccorso F, Tan P H, Rozhin A G and Ferrari A C 2009 Nanotube-polymer composites for ultrafast photonics *Adv. Mater.* **21** 3874–99
[13] Bao Q, Zhang H, Wang Y, Ni Z, Yan Y, Shen Z X, Loh K P and Tang D Y 2009 Atomic-layer graphene as a saturable absorber for ultrafast pulsed lasers *Adv. Funct. Mater.* **19** 3077–83
[14] Sun Z, Hasan T, Torrisi F, Popa D, Privitera G, Wang F, Bonaccorso F, Basko D M and Ferrari A C 2010 Graphene mode-locked ultrafast laser *ACS Nano* **4** 803–10
[15] Lin G-R and Lin Y-H 2012 Toward cheaper fiber laser pulses *SPIE Newsroom* (https://doi.org/10.1117/2.1201204.004185)
[16] Gao L, Zhu T and Zeng J 2014 Wavelength spacing tunable, multiwavelength Q-switched mode-locked laser based on graphene-oxide-deposited tapered fiber (https://doi.org/ arXiv:1401.1299v1 [physics.optics])
[17] Wang F, Drzal L T, Qin Y and Huang Z 2015 Mechanical properties and thermal conductivity of graphene nanoplatelet/epoxy composites *J. Mater. Sci.* **50** 1082–93
[18] Lin Y-H and Lin G-R 2012 Free-standing nano-scale graphite saturable absorber for passively mode-locked erbium-doped fiber ring laser *Laser Phys. Lett.* **9** 398–404
[19] Lin Y-H, Yang C-Y, Liou J-H, Yu C-P and Lin G-R 2013 Using graphene nano-particle embedded in photonic crystal fiber for evanescent wave mode-locking of fiber laser *Opt. Express* **21** 16763–76
[20] Hamra A A B, Lim H N, Chee W K and Huang N M 2016 Electro-exfoliating graphene from graphite for direct fabrication of supercapacitor *Appl. Surf. Sci.* **360** 213–23

[21] Lai Q, Zhu S, Luo X, Zuo M and Huang S 2012 Ultraviolet-visible spectroscopy of graphene oxides *AIP Advances* **2** 032146
[22] Ferrari A C 2007 Raman spectroscopy of graphene and graphite: disorder, electron-phonon coupling, doping and nonadiabatic effects *Solid State Commun.* **143** 47–57
[23] Ferrari A C and Robertson J 2000 Interpretation of Raman spectra of disordered and amorphous carbon *Phys. Rev.* B **61** 14095
[24] Ferrugiari A, Tommasini M and Zerbi G 2015 Raman spectroscopy of carbonaceous particles of environmental interest *J. Raman Spectrosc.* **46** 1215–24
[25] Sobon G, Sotor J, Jagiello J, Kozinski R, Zdrojek M, Holdynski M, Paletko P, Boguslawski J, Lipinski L and Abramski K M 2012 Graphene oxide versus reduced graphene oxide as saturable absorbers for Er-doped passively mode-locked fiber laser *Opt. Express* **20** 19463–73
[26] Thomsen C and Reich S 2000 Double resonant Raman scattering in graphite *Phys. Rev. Lett.* **85** 5214
[27] Gupta A, Chen G, Joshi P, Tadigadapa S and Eklund P C 2006 Raman scattering from high-frequency phonons in supported n-graphene layer films *Nano Lett.* **6** 2667–73
[28] Martinez A, Fuse K, Xu B and Yamashita S 2010 Optical deposition of graphene and carbon nanotubes in a fiber ferrule for passive mode-locked lasing *Opt. Express* **18** 23054–61
[29] Bao Q, Zhang H, Ni Z, Wang Y, Polavarapu L, Shen Z, Xu Q-H, Tang D and Loh K P 2011 Monolayer graphene as a saturable absorber in a mode-locked laser *Nano Res.* **4** 297–307
[30] Chen H-R, Tsai C-Y, Cheng H-M, Lin K-H and Hsieh W-F 2014 Passive mode locking of ytterbium- and erbium-doped all-fibers using graphene oxide saturable absorbers *Opt. Express* **22** 12880–9
[31] Guo B, Yao Y, Xiao J-J, Wang R-L and Zhang J-Y 2016 Topological insulator-assisted dual-wavelength fiber laser delivering versatile pulse patterns *IEEE J. Sel. Top. Quantum Electron.* **22** 8–15
[32] Khazaeinezhad R, Kassani S H, Jeong H, Nazari T, Yeom D-I and Oh K 2015 Mode-locked all-fiber lasers at both anomalous and normal sispersion regimes based on spin-coated $MoS_2$ nano-sheets on a side-polished fiber *IEEE Photon. J.* **7** 1–9
[33] Ge Y *et al* 2016 Revision on fiber dispersion measurement based on Kelly sideband measurement *Microw. Opt. Technol. Lett.* **58** 242–5
[34] Liu H H, Chow K K, Yamashita S and Set S Y 2013 Carbon-nanotube-based passively Q-switched fiber laser for high energy pulse generation *Opt. Laser Technol.* **45** 713–6
[35] Sobon G, Sotor J, Pasternak I, Strupinski W and Abramski K 2014 Graphene-based, ultrafast Er-doped fiber laser with linearly polarized output pulses *Photon. Lett. of Poland* **6** 65–7
[36] Luo A-P, Liu H, Zhao N, Zhang X-W, Liu M, Tang R, Luo Z-C and Xu W-C 2014 Observation of three bound states from a topological insulator mode-locked soliton fiber laser *IEEE Photon. J.* **6** 1–8
[37] Meng Y, Zhang S, Li X, Li H, Du J and Hao Y 2012 Multiple-soliton dynamic patterns in a graphene mode-locked fiber laser *Opt. Express* **20** 6685–92
[38] Kashiwagi K and Yamashita S 2009 Deposition of carbon nanotubes around microfiber via evanescent light *Opt. Express* **17** 18364–70
[39] Woodward R I, Kelleher E J R, Howe R C T, Hu G, Torrisi F, Hasan T, Popov S V and Taylor J R 2014 Tunable Q-switched fiber laser based on saturable edge-state absorption in few-layer molybdenum disulfide ($MoS_2$) *Opt. Express* **22** 31113–22
[40] Yu H, Zheng X, Yin K, Cheng X and Jiang T 2016 Nanosecond passively Q-switched thulium/holmium-doped fiber laser based on black phosphorus nanoplatelets *Opt. Mater. Express* **6** 603–9